Course No.: ME 498

SIMULATION OF DIFFERENT NOSE SHAPES OF HYPERSONIC VEHICLE TO MINIMIZE BOTH DRAG AND HEAT TRANSFER

A thesis proposal is submitted in partial fulfillment of the requirements for thedegree of

Bachelor of Science

In

Mechanical Engineering

Submitted by

Jamil Hossain

Student ID: 1803102

Supervised By: Prof. Dr. Sheikh Muhammad Humayun Kabir

Professor

Department of Mechanical Engineering

Chittagong University of Engineering & Technology

Chattogram-4349, Bangladesh

CHITTAGONG UNIVERISTY OF ENGINEERING AND TECHNOLOGY, CHATTOGRAM

(PROJECT AND THESIS)

COURSE NO.: ME 498

Title of the Project: Simulation of different nose shapes of hypersonic vehicle to minimize both drag and heat transfer.

Name of the Student: Jamil Hossain

Student ID: 1803102 **Session:** 2021-2022

Cell phone no: 01878566963

Name of the Department: Mechanical Engineering **Program:** B. Sc. Engg.

Name of the Supervisor: Prof. Dr. Sheikh Muhammad Humayun Kabir
Professor
Department of Mechanical Engineering, CUET

Signature of the Student

Signature of the Supervisor

Abstract

The goal of this work is to select a nose shape among the chosen few that provide reduced drag and heat transfer during hypersonic flight. The selected shapes are bi-conic, elliptical and parabolic nose. Since, two of the major difficulties incorporated in bodies travelling at hypersonic speed are high magnitude of drag and heat transfer. Reducing them is of high importance while designing an aircraft. Developing such a shape is challenging due to their conflicting relationship with nose shape i.e. a shape reducing high amount of drag also enhances heat transfer and vice versa. So, those nose shapes are designed and analyzed by a computational fluid dynamics (CFD) software. Engineering simulation software ANSYS is used to solve Reynolds-averaged Navier-Stokes (RANS) equations along with k-ω SST turbulence model to analyze the three selected nose shapes at a Mach no. of 7.1 at an altitude of 10 km from sea-level. At the end of the simulation, the comparison of the results shown concluded the parabolic nose as the best performer than others.

Acknowledgement

All credits go to the Almighty, for his boundless grace in successful completion of this thesis. At the very beginning I express my sincere gratitude and profound indebtedness to my thesis supervisor Prof. Dr. Sheikh Muhammad Humayun Kabir, Professor, Department of Mechanical Engineering, CUET, Chittagong-4349, under whose continuous supervision, this thesis proposal is carried out. His affectionate guidance, valuable suggestions and inspirations throughout this work made this study possible.

Author

Jamil Hossain

Table of Contents

List of Figures

List of Tables

Chapter 1

Introduction

1.1 Introduction

Designing hypersonic vehicle is one of greatest challenges for engineers as it includes various fields of scientific knowledge like aerodynamics, heat transfer, chemistry etc. Combining all those distinct fields of knowledge while designing are both complex and challenging for engineers. That is why this particular field has so much to offer to interested people to explore exciting and all new possibilities.

1.2 Background

The idea of "faster and higher," which has always been the driving force behind aviation, was what allowed the Wright brothers' 35 mph sea level flights in 1903 and the exponential development to the human space travel missions of the 1960s and 1970s. The present-day records for altitude and speed of manned flight are the moon and 36,000 ft/s, which is more than 36 times the speed of sound. These records were achieved by the Apollo lunar capsule in 1969. Reentering the atmosphere after the Apollo mission's lunar mission was over was one of its most important parts, despite the fact that most of it took place in space, far from the earth's atmosphere. Hypersonic aerodynamics is the study of the aerodynamic effects of very fast flight, such as those that occur during atmospheric reentry. In addition to manned and unmanned reentry vehicles, NASA is also looking at the possibility of a hypersonic travel. Ramjet-powered hypersonic weapons are another potential use for this technology that the military is now studying. [1].

1.3 Hypersonic flow and it’s characteristics

Hypersonic flow is loosely defined as the flow in which Mach number is greater than 5.

The reason why hypersonic flows at high Mach umber are different from those of lower Mach number supersonic flows due to their distinct characteristics.

Some of those are-

- Shock and boundary layer interaction.
- High temperature in the shock layer.
- High pressure drag.
- Dissociation and ionization of air.

These distinct characteristics made aerodynamic design of a hypersonic vehicle more complex and challenging. Since, the main objective of this project is to minimize both drag and heat transfer, the preceding discussions will be focused on those two matters only.

1.4 How to reduce drag?

Aerodynamic drag can be divided into two components: pressure drag and friction drag. Pressure drag occurs because the leading edge or nose of the body experiences large pressures due to shock waves, and the tailing edge of the body experiences smaller pressures due to expansion waves. Summing these pressures over the area of the body gives a net force opposite to the direction of motion. Friction drag occurs primarily due to the velocity gradient in the boundary layer next to the wall. A turbulent boundary layer has a larger velocity gradient than a laminar boundary layer and therefore imparts a higher skin friction drag on thebody. Combining wave drag with pressure drag and skin friction, the drag on a hypersonic vehicle with a turbulent boundary layer is quite large. Wave drag, pressure drag, and skin friction are all combined to provide a significant amount of drag on a hypersonic vehicle in a turbulent boundary layer. From the equation of total drag, we get

$$D = \frac{1}{2} C_D \rho A V^2$$

Here,

C_D= Drag Coefficient

ρ = Freestream Density

A= Reference Area

V= Freestream Velocity

Considering a body moving at a given altitude, air density, freestream velocity and reference area are fixed. Only parameter that can be changed is C_D. ReducingC_D, while maintaining a constant reference area can only be obtained by varying shape of the leading edge of the vehicle. Using a pointy leading edge or nose reduces drag as it weakens the shock wave. Weaker shock wave generates smaller pressure drag which is the dominating drag component at supersonic and hypersonic velocities.

1.5 How to reduce heat transfer?

The phenomenon of aerodynamic heating causes heat transfer at hypersonic speeds. Large amounts of kinetic energy present in the freestream are transformed into thermal energy as molecules move through the shock wave. The idea of the amount of the thermal energy conversion from kinetic energy can be easily predicted recalling the magnitude of the velocity of the vehicle. Then the thermal energy is transferred from the shock layer to the vehicle's body. Such immense heat energy is capable of melting down the vehicle components. To reduce body heating, a blunt nose shape is preferred as it creates stronger shock wave which disperse the heat into the airflow over the body as shown in Fig-01.

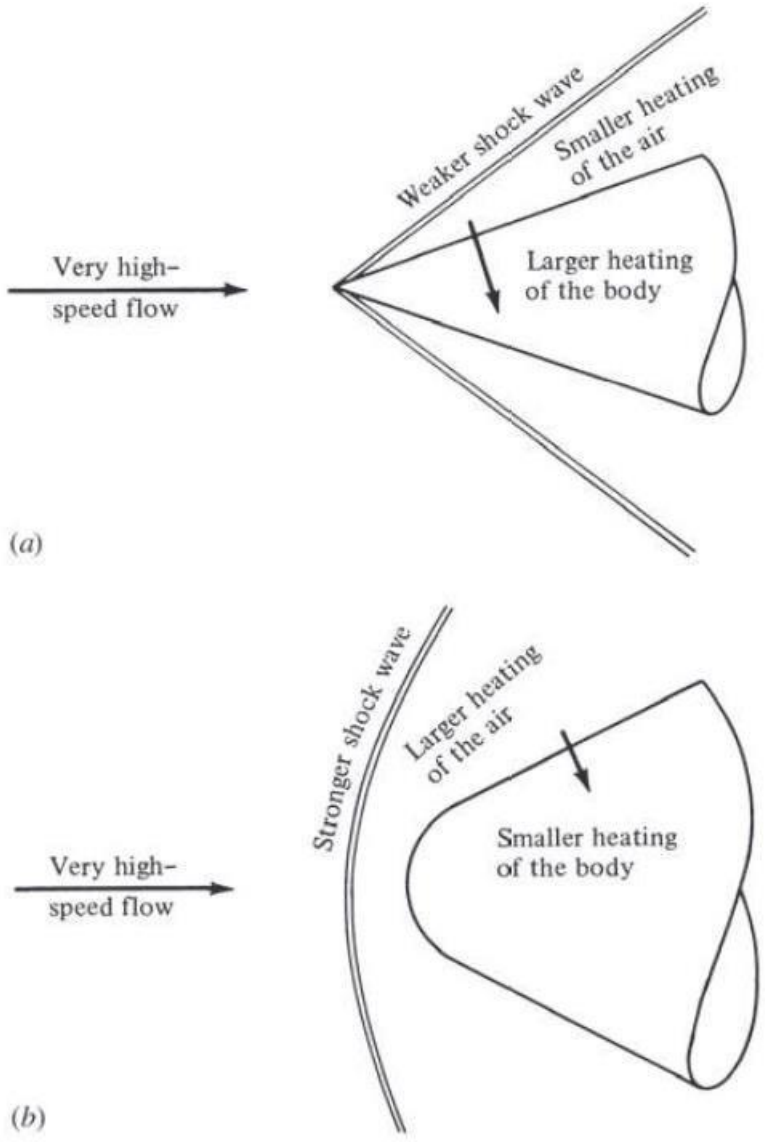

Figure 1.1 Contrast of aerodynamic heating for slender and blunt vehicles. [1]

(a) Slender body. (b) Blunt body

1.6 Objective

- Simulation of different nose shapes for hypersonic vehicle.
- To select a nose shape that provides reduced drag and heat transfer compared to the others.

1.7 Why simulation is chosen?

Due to unavailability and high costing of hypersonic wind-tunnel, ground routine testing is impractical and the experimental data from actual testing are challenging and difficult to obtain. Avoiding those difficulties, CFD simulation technology provide such a relieving alternative in hypersonic vehicle designing. That is why we choose simulation for our work.

Chapter 2
Literature Review

2.1 Introduction

There can be found a great deal of work where different methods and techniques are employed to reduce aerodynamic drag and heating of bodies travelling at hypersonic speed. For example, aero-spike, counter-flow injection, energy deposition and surface coating are some of them. There can also be found various works on individually minimizing drag and heat transfer only. But for our work here, we are interested in developing a nose shape only that minimizes both drag and heat transfer simultaneously.

2.2 Previous work

Our objective is to reduce both aerodynamic drag and heating of hypersonic vehicle via suitable nose shape selection. There was found only one previous work that includes all the features of our work. By combining a genetic algorithm with CFD software, Christopher Seager and Ramesh

K. Agarwal have discovered optimum designs for an axisymmetric blunt body that have the least amount of drag and heat flow [2].

In supersonic and hypersonic flows, A. Hemateja, B. R. Teja, A. D. Kumar, and S. Rakesh discovered a relationship between nose radius and drag. They also discovered that the task at hand may determine the ideal nose radius value because increasing nose radius decreases heat transfer but increases drag, and vice versa [3].

A novel non-ablative thermal protection system for hypersonic vehicles based on flow field reconstruction has been shown to successfully reduce drag and aerodynamic heating. Yunfeng Liu and Zonglin Jiang proposed this new concept with experimental and numerical results indicating promising engineering applications [4].

To lessen drag and transfer of heat, Shi-bin Li, Wei Huang, Jing Lei, and Zhenguo Wang devised and quantitatively evaluated the porous opposing jet approach. This work demonstrates that by combining the porous opposing jet design with variable blunt techniques, the aerodynamic performance may be further enhanced. The size of the Mach disk and the off-distance of the shock wave decrease with an increase in the number of jet orifices(N) when N

is odd. When N is equal, the high temperature area will shrink as N rises. When N is odd, the drag reduction ratio rises as the number of jet orifices grows. When N is even, though, the tendency is the opposite. In addition, when N is odd, the impact of drag decreaseis better than when N is even [5].

K. Mansour and M. Khorsandi has shown that high drag and heat load can be reduced during hypersonic flight by placing an aero spike on the front of a blunt nose cone, and the computed shock stand-off distance in this study is reasonably consistent with previous works in the field. They used numerical simulation to model hypersonic flow with a Mach number of 6 around a spike. For the purpose of calculating the associated Reynolds Average Navier-Stoke equations, the conventional k-e model was employed. The calculated findings demonstrate that the studded blunt body's drag coefficient is lower than that of a body without spikes. Additionally, their numerical calculations and related experimental studies agree. Additionally, there is fair agreement between the computed shock stand-off distance and otherrelated works [6].

The computational analysis by Tahani et al. reveals that aerodisk is superior than aerospikesin terms of effectiveness. For spikes of varying lengths, shapes, and combinations, the numerical solution has been tested. Various bow shocks, such as spikeless, conical, flat, and hemispherically mounted aerodisks, can be produced by further modifying the spike's tip. Unsteady compressible 3-D Navier-Stokes equations are resolved for a flow through a forward-facing spike attached to a heat shield at a free stream Mach number of six using the k (SST) turbulence model. An appropriate degree of verification is reached when the numerical findings obtained are contrasted with the experimental ones. The aerodisk outperforms the aerospike in this analysis. The innovations lowered wall temperature responses by 15% and by 60%, respectively, and reduced drag by 60% [7].

Using a forward-facing jet, Benjamin Meyer, H. Nelson, and D. Riggins demonstrated a numerical analysis to minimize drag and heat transmission. A two-dimensional numerical analysis of the effects of a forward-facing jet positioned at the stagnation point of a blunt body on wave drag, heat transfer, and skin-friction drag is shown for a Mach 6.5 flow at 30 km altitude. The entire set of Navier-Stokes equations is used when the viscosity and thermal conductivity are changed. Upstream injection has a significant impact on the flow field. It may be possible to significantly reduce drag and heat transmission under the correct jet circumstances, which might increase the volumetric efficiency and static stability of aircraft and lessen the requirement for thermal shielding for hypersonic vehicles. [8]

2.3 Problem statement

The discussion above clarifies that there has been some good amount of work done regarding drag and heating reduction of hypersonic bodies. But those were achieved by means of additional extension to the body like protective coating for heat reduction and mounting aerospike and others to reduce drag. Even those methods only deal with one concern either drag or heating. But if there could be a process that would reduce both of those concerns simultaneously that will be a suitable nose shape design. That could not only deal with both concerns at once, but also saves the trouble of additional work of coating and aerospike adjusting.

Chapter 3

Research Methodology

3.1 Introduction

Our goal in this work is to analyze different nose shapes and choose the best option that provide minimum drag and heat transfer to the body. To achieve that goal, we have to go through processes like shape development, simulation etc. For the ease of implementation and understanding, the entirety of those processes is divided into three major parts. Those are-

a. Nose selection and design.
b. Body meshing.
c. CFD Simulation.

A process flow diagram is shown below.

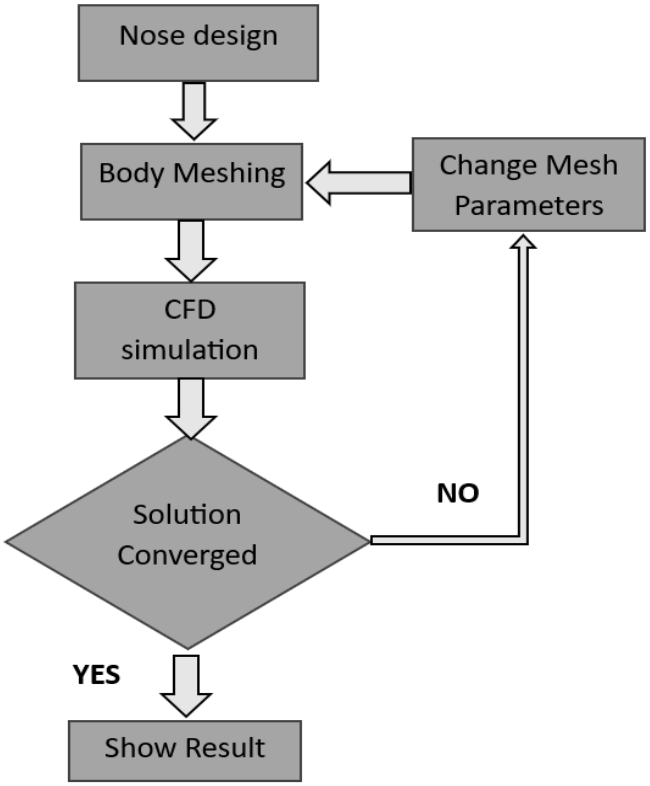

Figure 3.1 Flow chart of the process.

3.2 Nose selection and design

The first step of our work is to generate nose profile. There exist various axisymmetric and non-axisymmetric shape of aerodynamic importance. But this work's concern doesn't include each and every of them as it was established in previous discussion that a pointy nose like conic

nose experience a large amount of meat transfer and a slender body like spherically blunted conic, spherically blunted ogive etc. experience a large amount of drag. By discarding those choices, three shapes of interest were chosen for this work. Those are-

- Bi-conic
- Elliptical
- Parabolic

After selecting some suitable shapes, they were generated with the help a CAD software named SOLIDWORKS. For the ease of analysis, generated shapes were designed with a fineness ratio of 2 i.e. nose length to base diameter ratio is 2. The generated shapes are shown below-

3.2.1 Bi-conic nose shape

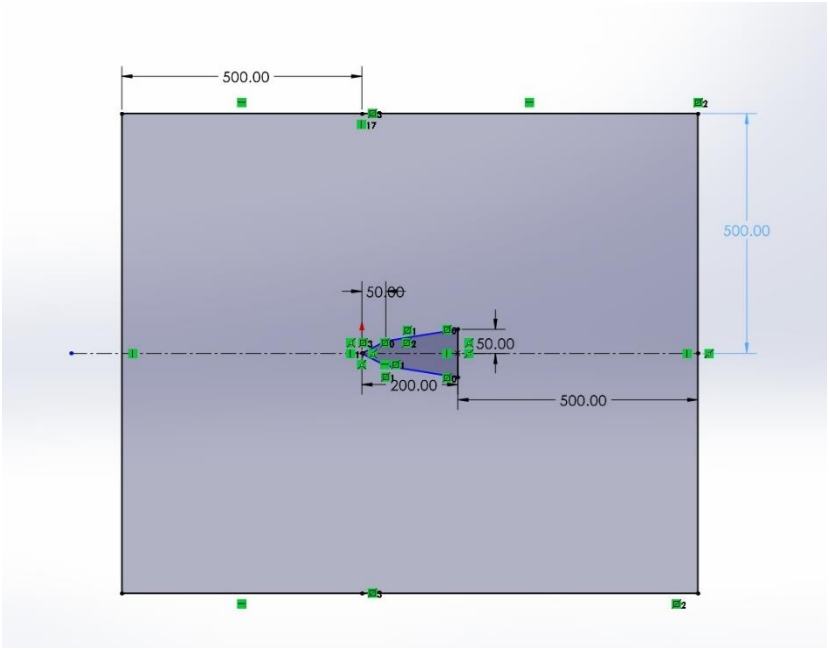

Figure 3.2 Bi-conic nose shape with dimensions.

Here in Figure 3.2, is the snapshot of a bi-conic nose with base diameter being 100 mm and nose length being 200 mm. It is designed in such a way that the first 50 mm of the length has cone more diverged than the one along the rest of the length.

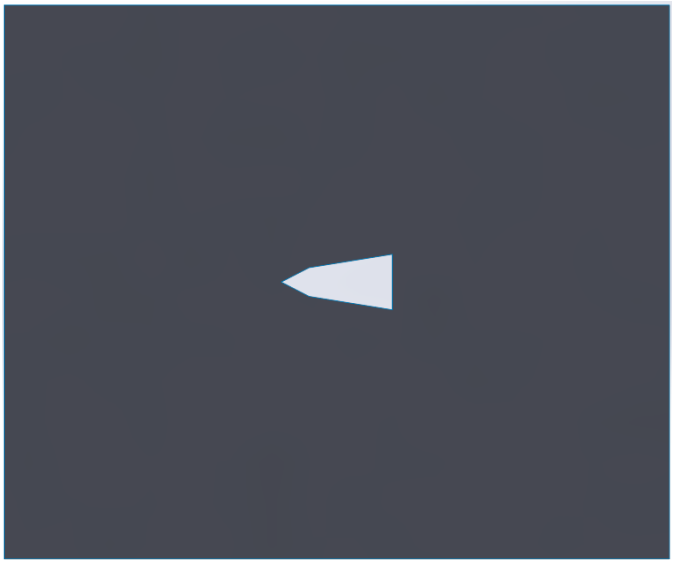

Figure 3.3 Generated solid body of bi-conic nose with boundaries.

This in Figure 3.3 is the snapshot of the generated solid body from the dimensions shown earlier. Since the study will be conducted on 2D nose cone, a 2D planar surface was generated.

3.2.2 Elliptical nose shape

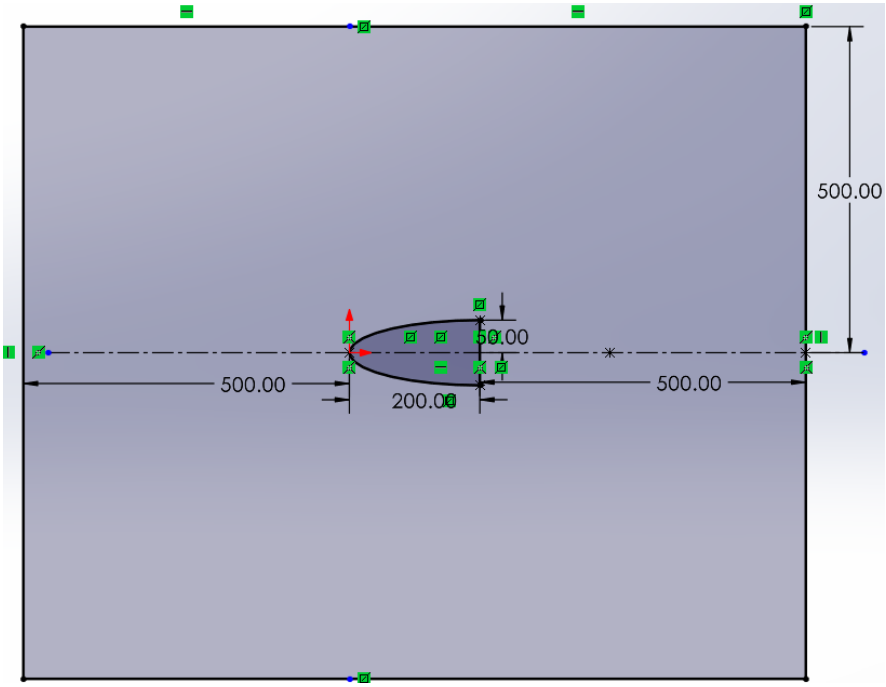

Figure 3.4 Elliptical nose shape with dimensions.

This in Figure 3.4 is a snapshot of the elliptical nose where length of the nose being along the major axis at a magnitude of 200 mm and nose diameter being along the minor of 100 mm.

Figure 3.5 Generated solid body of elliptical nose with boundaries.

This in Figure 3.5 is the snapshot of the generated solid body from the dimensions shown earlier. Since the study will be conducted on 2D nose cone, a 2D planar surface was generated.

3.2.3 Parabolic nose shape

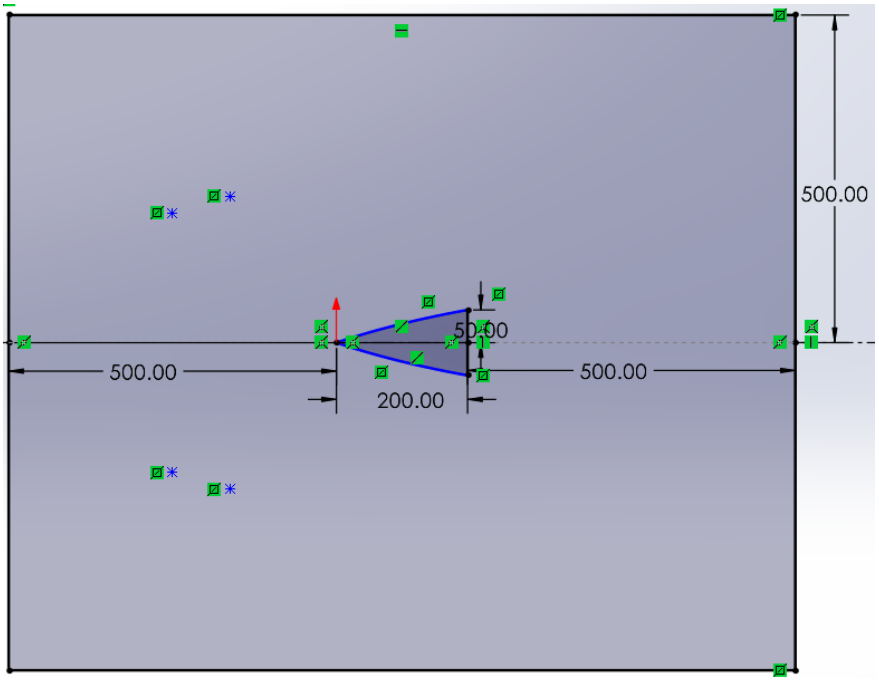

Figure 3.6 Parabolic nose shape with dimensions.

The parabolic nose shown in Figure 3.6 was designed by stripping out the symmetric upper and lower parts and merging them into one single body. That is why the nose front appears as pointy rather than a smooth curved profile of a parabola.

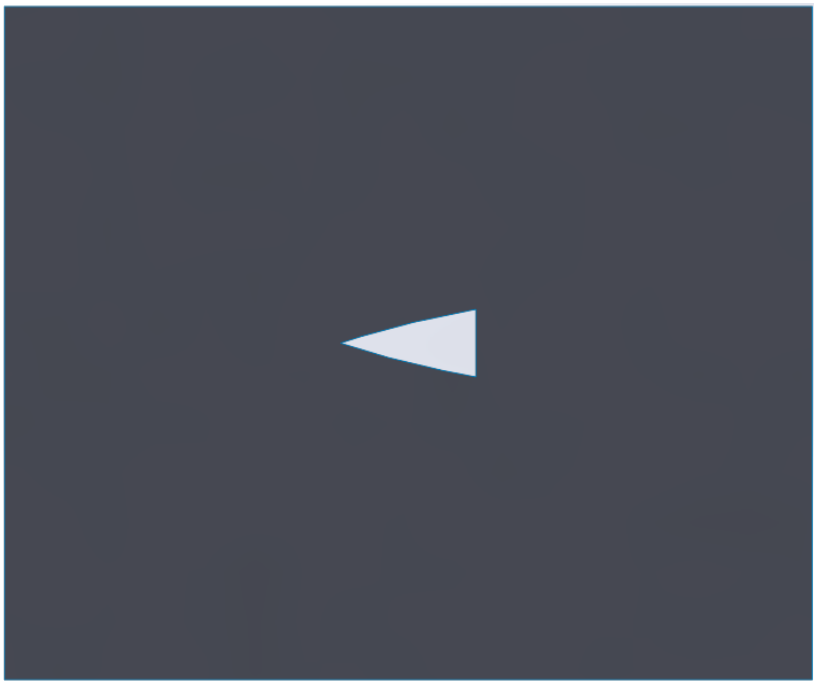

Figure 3.7 Generated solid body of parabolic nose with boundaries.

This in Figure 3.7 is the snapshot of the generated solid body from the dimensions shown earlier. Since the study will be conducted on 2D nose cone, a 2D planar surface was generated.

3.3 Body meshing.

Following the creation of the nose shape, it is parameterized and loaded into the ICEM (Integrated Computer-aided Engineering and Manufacturing) meshing program. This creates a mesh around the body shape. For this and the next simulation work, the engineering simulation program ANSYS will be utilized. To more correctly approximate heat transport, a mesh with a high density of cells will be constructed close to the wall. Without compromising the solution's accuracy, cell density of meshing can be reduced outside of the shock zone and beyond the boundary layer.

To ensure good mesh quality, some quality measuring parameters should be maintained within acceptable ranges. Those parameters are-

3.3.1 Aspect ratio

It represents the stretching of a cell. It is defined as the maximum ratio of distances of face centroid to body centroid and node to body centroid of a cell. Though a magnitude of 1 represents the best aspect ratio but 1 to 5 is the acceptable limit [10].

3.3.2 Jacobian ratio

It is a measure that represents whether an element is self-intersecting or not. The acceptable range is between 1 to 10 [9].

3.3.3 Skewness

It represents whether an element is equilateral and equiangular or not. The acceptable range for skewness is 0 to 0.5 [10].

The generated mesh along with quality parameters for the selected shapes are shown below.

3.3.4 Bi-conic body mesh

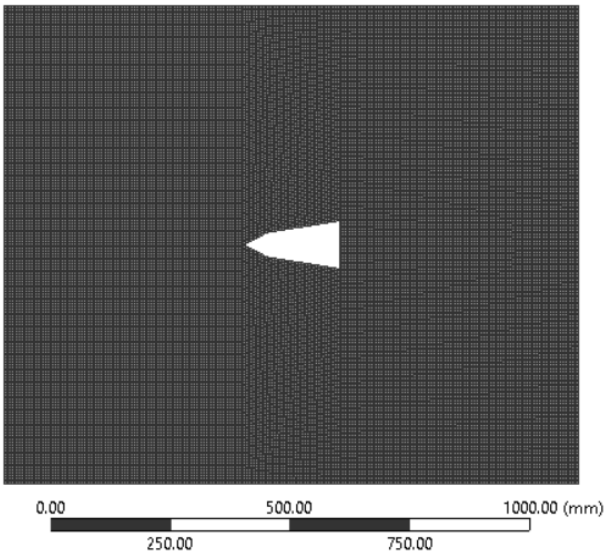

Figure 3.8 Bi-conic meshed body.

This in Figure 3.8 is a snapshot of bi-conic meshed body of element size 5 mm with 48282 nodes and 47790 elements. For the analysis, element size of 4,6 and 7 mm were also generated.

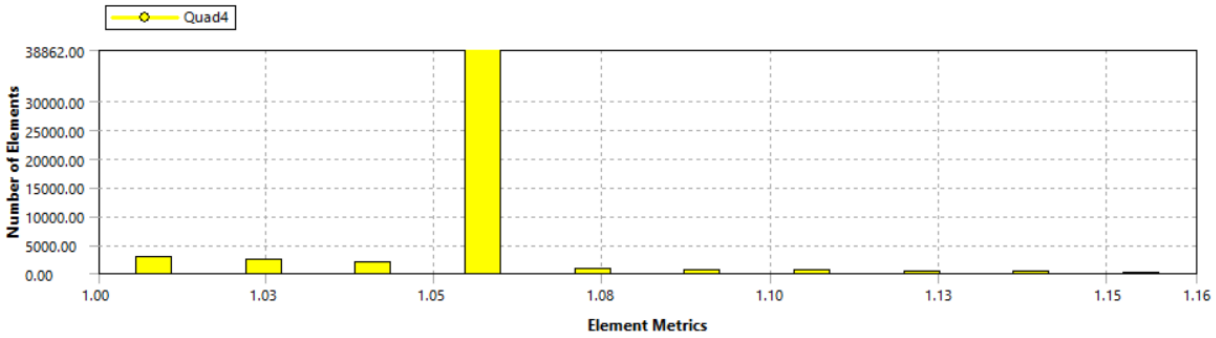

Figure 3.9 Aspect ratio of Bi-conic meshed body.

Here in Figure 3.9, it can be seen that aspect ratio of elements from generated meshed body varies from 1 to 1.16 which is within the tolerable range mentioned earlier i.e. below 10.

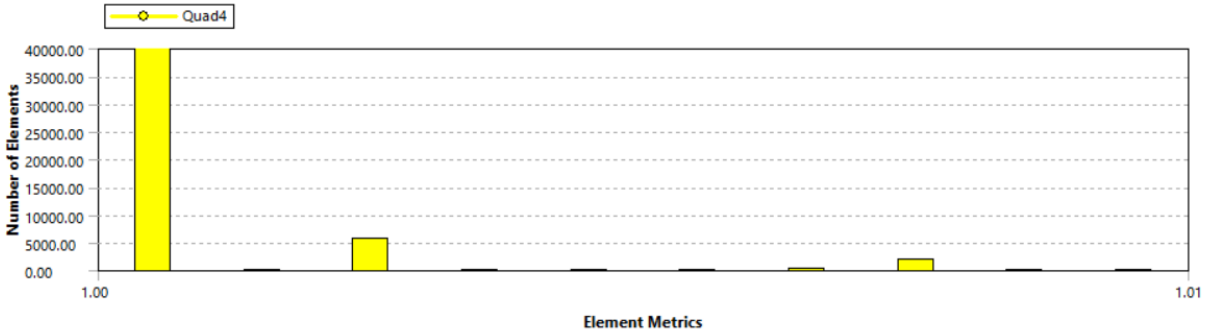

Figure 3.10 Jacobian ratio of Bi-conic meshed body.

In Figure 3.10, it can be seen that the Jacobian ratio of the elements of the generated meshed body varies from 1 to1.01 which is in the tolerable range i.e. 1 to 5.

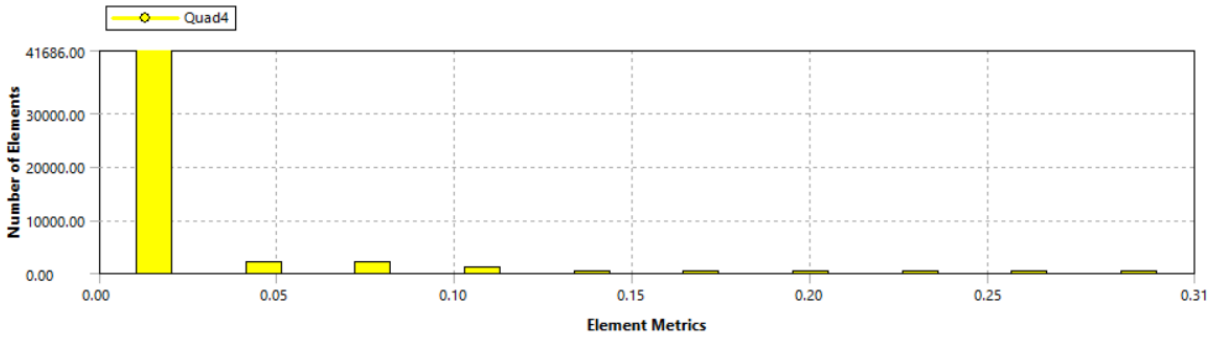

Figure 3.11 Skewness of Bi-conic meshed body.

Skewness of elements of the generated meshed body varies from 0 to 0.31 as shown in Figure 3.11 which is within tolerable range mentioned earlier i.e. 0 to 0.5.

3.3.5 Elliptical meshed body

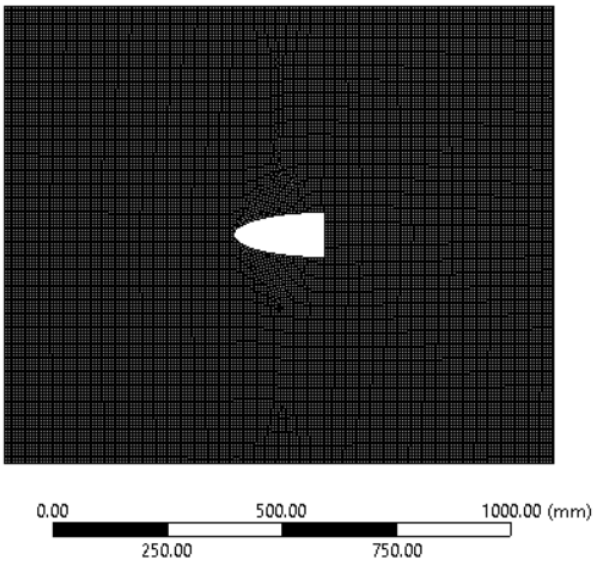

Figure 3.12 Elliptical meshed body.

This in Figure 3.12 is a snapshot of elliptical meshed body of element size 6 mm with 33436 nodes and 33029 elements. For the analysis, element size of 5 and 7 mm were also generated.

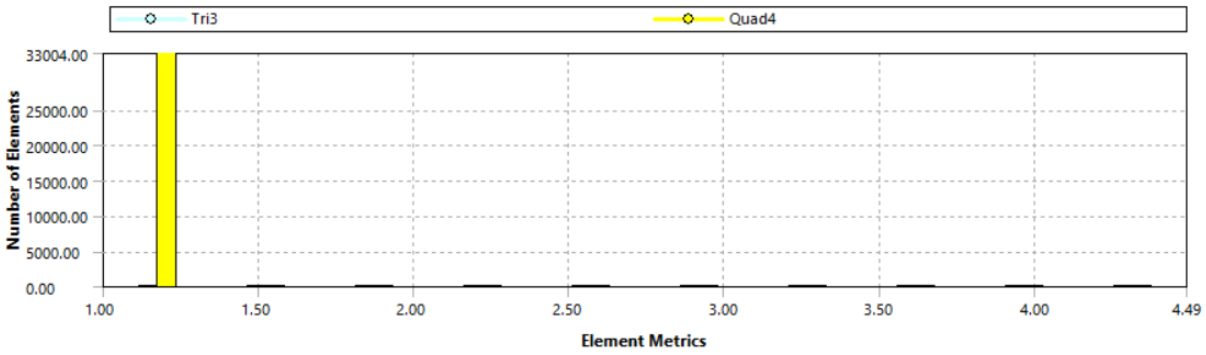

Figure 3.13 Aspect ratio of elliptical meshed body.

Here in Figure 3.13, it can be seen that aspect ratio of elements from generated meshed body varies from 1 to 4.49 which is within the tolerable range mentioned earlier i.e. below 10.

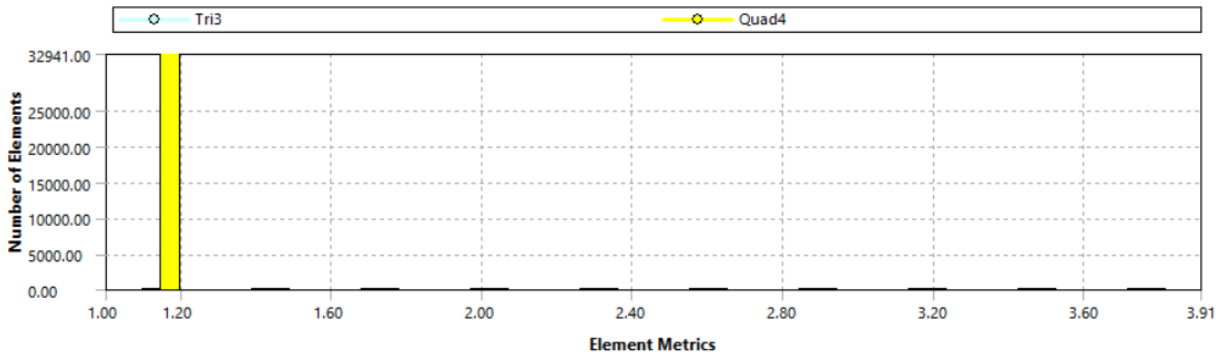

Figure 3.14 Jacobian ratio of elliptical meshed body.

The Jacobian ratio of the elements of the generated meshed body varies from 1 to 3.91 as shown in Figure 3.14 which is in the tolerable range i.e. 1 to 5.

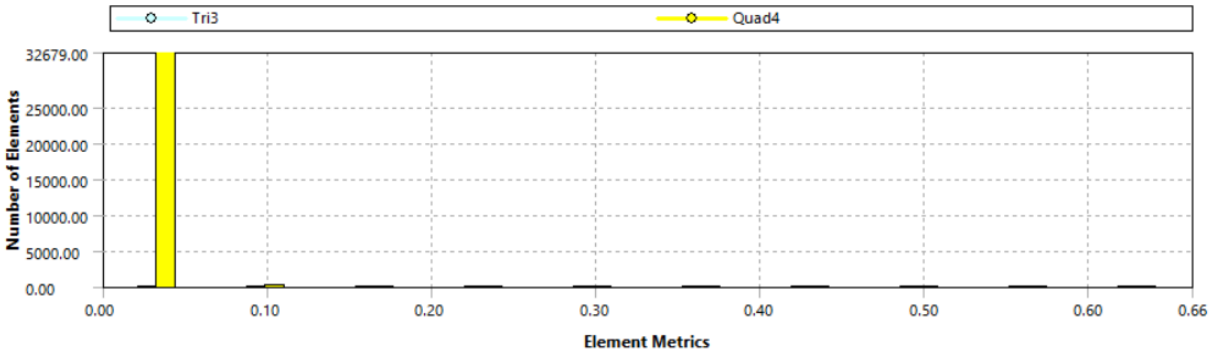

Figure 3.15 Skewness of elliptical meshed body.

Skewness of elements of the generated meshed body varies from 0 to 0.66 as shown in Figure 3.15 which may not be within the tolerable range mentioned earlier i.e. 0 to 0.5, but the number of elements above skewness 0.5 is very few.

3.3.6 Parabolic body mesh

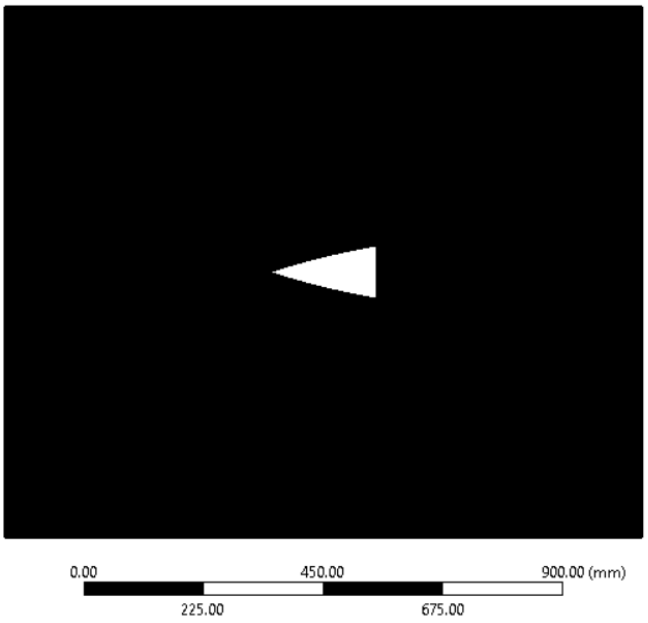

Figure 3.16 Parabolic meshed body.

This in Figure 3.16 is a snapshot of parabolic meshed body of element size 7 mm with 388000 nodes and 389400 elements. For the analysis, element size of 6,8 and 9 mm were also generated.

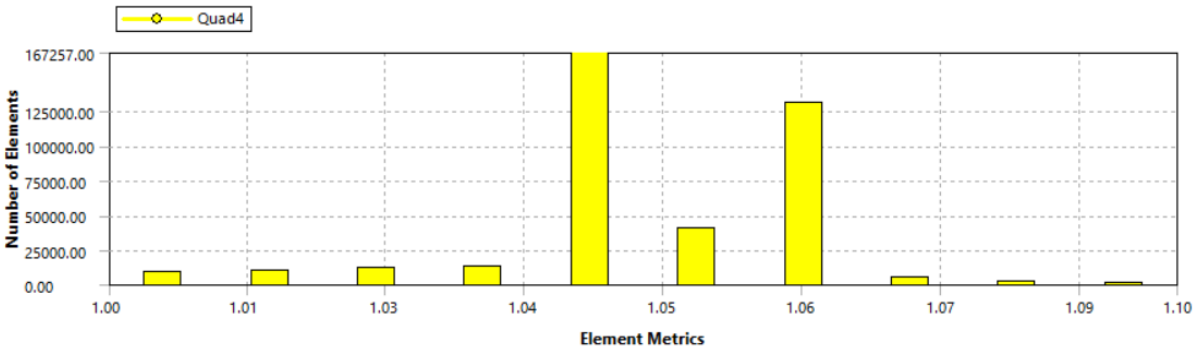

Figure 3.17 Aspect ratio of parabolic meshed body.

Here in Figure 3.17, it can be seen that aspect ratio of elements from generated meshed body varies from 1 to 1.10 which is within the tolerable range mentioned earlier i.e. below 10.

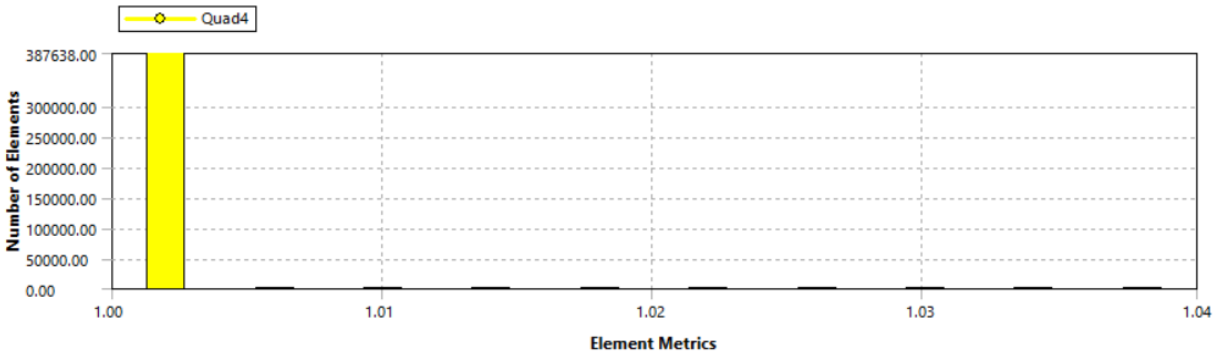

Figure 3.18 Jacobian ratio for parabolic meshed body.

The Jacobian ratio of the elements of the generated meshed body varies from 1 to 1.04 as shown in Figure 3.18 which is in the tolerable range i.e. 1 to 5.

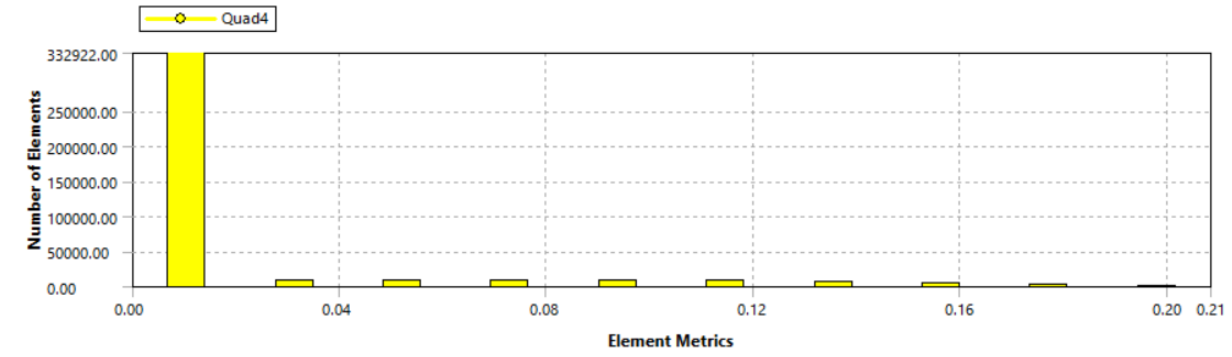

Figure 3.19 Skewness of parabolic meshed body.

Skewness of elements of the generated meshed body varies from 0 to 0.2 as shown in Figure 3.19 which is within tolerable range mentioned earlier i.e. 0 to 0.5.

3.4 CFD Simulation

The commercial CFD application ANSYS Fluent is used to load the mesh body. To determine the flow field and surface properties including skin friction, wall pressure coefficient, a total surface heat flux, Fluent solves the unstable compressible RANS (Reynold-averaged Navier-Stokes) equations in combination with the SST (Shear-stress transport) k-ω turbulence model. For the simulation, at first some parametric values need to be determined.

In this study, it was considered that the body is traveling at hypersonic speed of Mach no. 7.1 at an altitude of 10 km. At that altitude, the operating parameters are as shown in Table-3.1.

Table 3.1 Atmospheric air properties at 10 km altitude [11].

Parameters	Values
Temperature(T)	223 K
Pressure(P)	2.65×10^4 Pa
Density	0.4135 kg/m^3
Dynamic viscosity	1.458×10^{-5} N s/m^2

So, the stagnation properties become

Stagnation pressure: $\frac{p_t}{p} = (1 + \frac{\gamma-1}{2} M^2)^{\frac{\gamma-1}{\gamma}}$ …….. (i)

Stagnation temperature: $\frac{T_t}{T} = 1 + \frac{\gamma-1}{2} M^2$ ……. (ii)

Here,

p_t= Stagnation pressure (Pa)

p, (Atmospheric pressure) = 26500 Pa

T_t = Stagnation temperature (K)

T, (Ambient temperature) = 223 K

γ, (Specific heat ratio) = 1.4

M, (Mach no.) = 7.1

Now, putting those values into the equation (i) and (ii), we get

$\frac{p_t}{26500} = [1 + \frac{(1.4-1)}{2} (7.1)^2]^{\frac{1.4-1}{1.4}}$

⇨ p_t=120063053.5 Pa

And,

$\frac{T_t}{223} = 1 + (\frac{1.4-1}{2}) (7.1)^2$

⇨ T_t =2471.286 K

3.5 Simulation Setup

Table 3.2 Fluent setup and initial values.

Solver type	Density based
Models	Energy (On) SST k-omega (Turbulence)
Material	Air (Obeys ideal gas law) • Viscosity (Sutherland law)
Boundary conditions	Inlet conditions: • Pressure inlet is chosen • Inlet gauge pressure: 120036553.5 Pa • Inlet total temperature: 2471.286 K Outlet conditions: • Pressure outlet is chosen • Outlet gauge pressure: 0 Pa
Spatial discretization	Gradient: Least square cell based Flow: Second order upwind Turbulence KE: Second order upwind Specific dissipation rate: Second order upwind

- k-omega SST model was selected because it predicts near wall behavior more accurately than other models which is necessary for heat transfer analysis of this study.
- Air is selected as the flow medium which obeys ideal-gas laws and the density was considered constant. But the viscosity was not considered constant and was assumed to change according to Sutherland law.
- As for the boundaries, pressure inlet and outlet were chosen as the flow considered is an external aerodynamic flow whereas velocity inlet and outlet choice were discarded it is usually used for internal flows.
- For precise understanding of the flow domain, the values of pressure and temperature was calculated stagnation property relationships and the atmospheric pressure was subtracted from stagnation pressure for gauge pressure.

Chapter 4
Result and Discussion

4.1 Introduction

As the computation processes discussed in the methodology section, the generated meshed bodies were run for simulation in Fluent. Ansys Fluent then solved and provided the desired results of drag and heat flux for those nose shapes. Those results were run for different element sizes and the results were cross-checked with reliable sources of previously published literatures.

4.2 Bi-conic nose results

The obtained results for bi-conic nose for different element sizes are tabulated below.

Table 4.1 Obtained results for various element sizes for bi-conic nose.

Element Size(mm)	Nodes	No. of elements	Drag (N)	Heat flux (W/m^2)
7	24738	24386	37927.431	390524
6	33336	32928	37988.932	389869.4
5	48282	47790	37927.431	470255.4
4	75504	74888	37634.470	281504.7

The values obtained against 4 mm elements size are selected as final result of this study. These values were cross-checked with experimental values of bi-conics at Mach 10 by Charles G. Miller III, published by NASA [12]. He measured heat transfer for bi-conic nose at different angle of attack. Since, in this study, angle of attack was 0^o that is why some of his obtained data are shown here.

Table 4.2 Experimental values for validation.

x/L	Qdot (W/m^2)
0.000	3.372E+05
0.247	1.956E+04
0.287	1.893E+04
0..328	1.839E+04

Here at x/L of 0.000 i.e. at the tip of the body, the amount of heat transfer is 3.372E+05 W/m^2 which is higher than the obtained value in this study obviously as these values were obtained for Mach 10 since higher Mach number results in lower shock region thus increasing body heating.

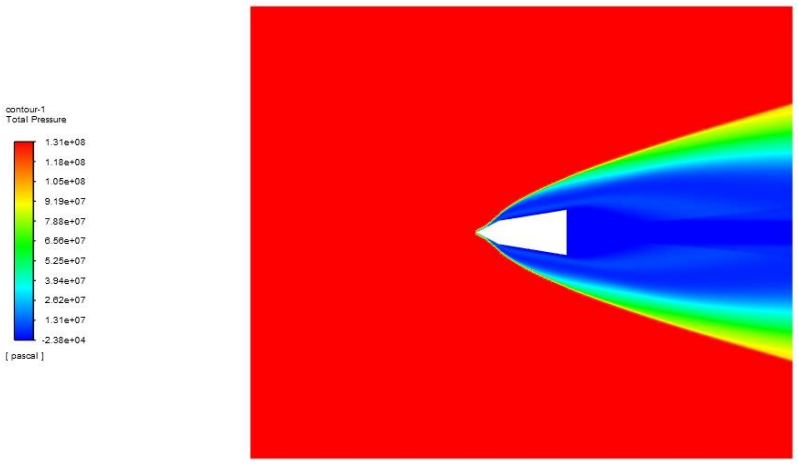

Figure 4.1 Pressure contour for bi-conic nose.

From the snapshot in Figure 4.1 of pressure contour for bi-conic nose, the sudden change in total pressure in front shock wave to behind the shock wave can be seen. That high amount of pressure change causes high amount of pressure drag.

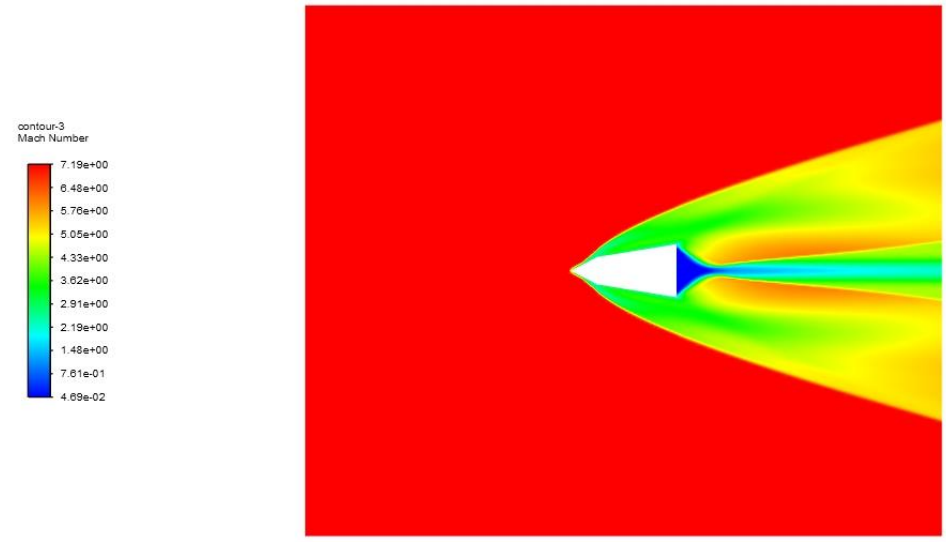

Figure 4.2 Velocity contour for bi-conic nose.

From the snapshot in Figure 4.2 of velocity contour, the change in velocity from the front to behind can be seen in terms of Mach number for the bi-conic nose. It can be seen from the red zoned area in front of the shock wave that it contains a high amount of kinetic energy which contributes to the body heating.

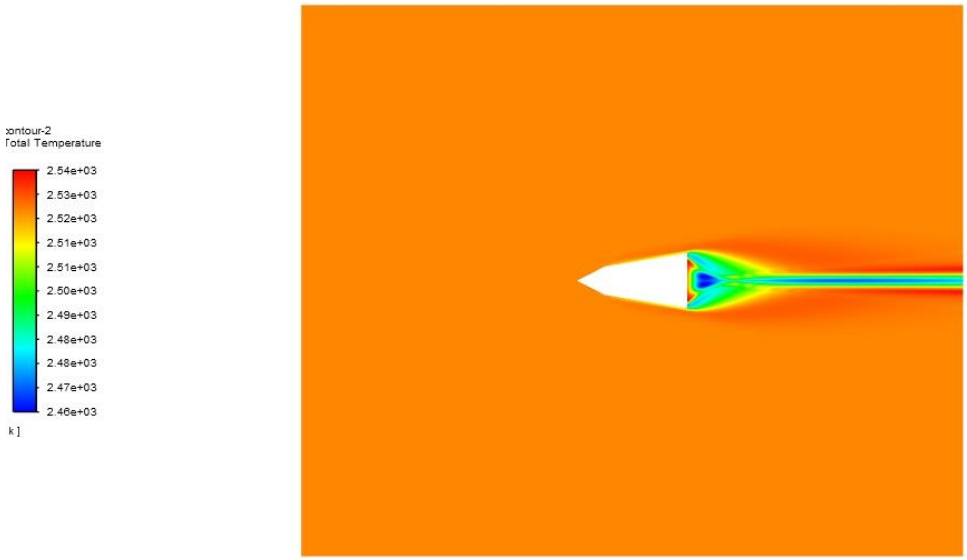

Figure 4.3 Temperature contour of bi-conic nose.

From the snapshot in Figure 4.3 of total temperature contour obtained due to the flow over bi-conic nose, it can be estimated that how much heat is being transferred to the body. The total temperature includes dynamic temperature which is a measure of kinetic energy contained by the freestream air. This kinetic energy than transformed into the thermal energy as air molecules passes through the shock wave.

4.2 Elliptical nose results

The obtained results for elliptical nose for different element sizes are tabulated in Table 4.3.

Table 4.3 Obtained results for various element sizes for elliptical nose.

Element size(mm)	Nodes	Elements	Drag (N)	Heat flux (W/m^2)
7	24587	24239	69007.439	643514.5
6	33436	33029	72428.46	690791.12
5	47905	47414	71580.91	712825.9

The value obtained against 5 mm element size is finalized here as result. These values were cross-checked with experimental values of elliptical nose at Mach 5.75 by Ashish Narayan et el. [13]. They obtained their results via numerical investigation of elliptical nose at different fineness ratio. Some of those values are tabulated in Table 4.4.

Table 4.4 Values obtained from literature for validation of elliptical nose.

Fineness ratio	Surface heat flux (W/m^2)
4.7	4.3E+05
3.6	3.55E+05
.8	3.51E+05
.6	3.48E+05

As it can be seen from the table above that the surface heat flux for fineness ratio of 2 would be between 3.51E+05 W/m^2 and 3.55E+05 W/m^2. But since the operating Mach number if this study is 7.1 then it can be said that the amount of heat transfer would much higher than this literature value at Mach 5.75.

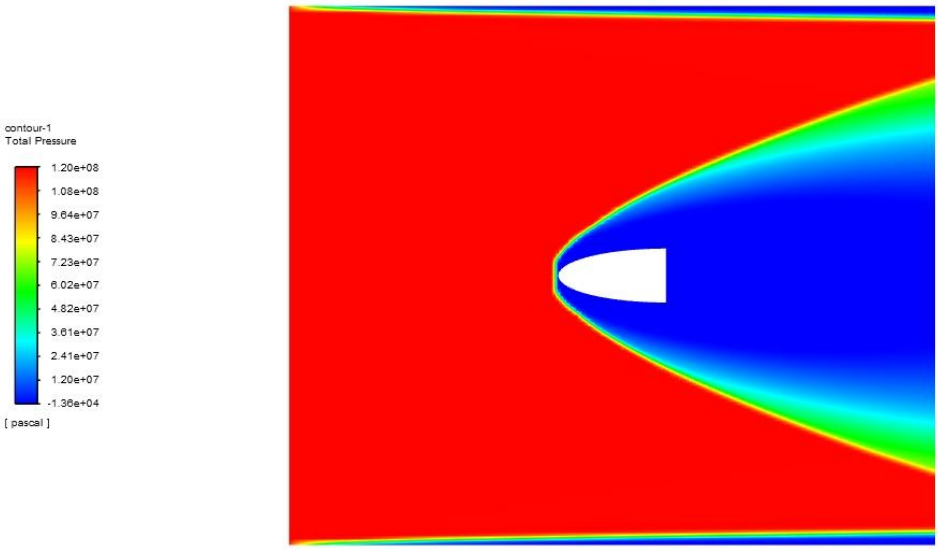

Figure 4.4 Pressure contour for elliptical nose.

From the snapshot in Figure 4.4 of pressure contour for elliptical nose, the sudden change in total pressure in front shock wave to behind the shock wave can be seen. That high amount of pressure change causes high amount of pressure drag. Also, it is evident from the snapshot that this nose creates a stronger shock wave which results in higher amount of drag.

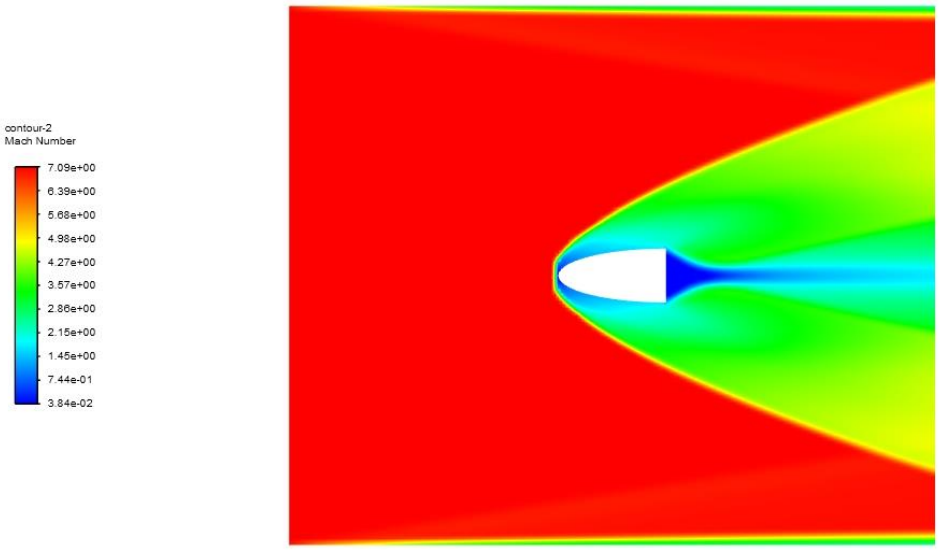

Figure 4.5 Velocity contour for elliptical nose.

From the snapshot in Figure 4.5 of velocity contour, the change in velocity from the front to behind can be seen in terms of Mach number for the bi-conic nose. It can be seen from the red

zoned area in front of the shock wave that it contains a high amount of kinetic energy which contributes to the body heating.

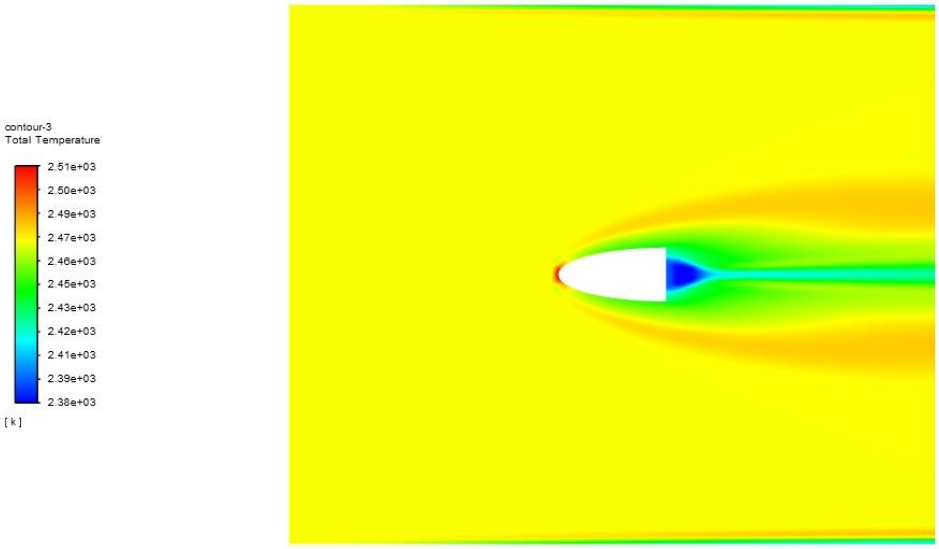

Figure 4.6 Temperature contour of elliptical nose.

From the snapshot in Figure 4.6 of total temperature contour obtained due to the flow over elliptical nose, it can be estimated that how much heat is being transferred to the body. The total temperature includes dynamic temperature which is a measure of kinetic energy contained by the freestream air. This kinetic energy than transformed into the thermal energy as air molecules passes through the shock wave.

4.3 Parabolic nose results

The obtained results for bi-conic nose for different element sizes are tabulated in Table 4.5.

Table 4.5 Obtained results for various element sizes for parabolic nose.

Element size(mm)	Nodes	Elements	Drag (N)	Heat flux (W/m^2)
9	240816	239712	23884.857	174336
8	305176	303936	23868.231	348415.98
7	388000	389400	23854.088	344064
6	528480	526848	23820.5116	257792

The values obtained for element size of 6 mm are finalized as results. These values were cross-checked with numerically investigated values of elliptical nose at Mach 5.8 by Ashish Narayan et el. [14]. Those values were obtained for parabolic nose shape at different fineness ratios. Some of the values are tabulated in Table 4.6.

Table 4.6 Values obtained from literature for validation of parabolic nose.

Fineness ratio	Surface heat flux(W/m^2)
4.7	6.3e+05
3.6	5.7e+05
1.2	2.3e+05
1.0	2.2e+05

From the table it can be seen that the heat flux for fineness ratio 2 will be between 2.3e+05 to 5.7e+05. Though the results obtained in the mentioned literature were against conditions slight different than this one's, but they give the idea of validity of this work's results.

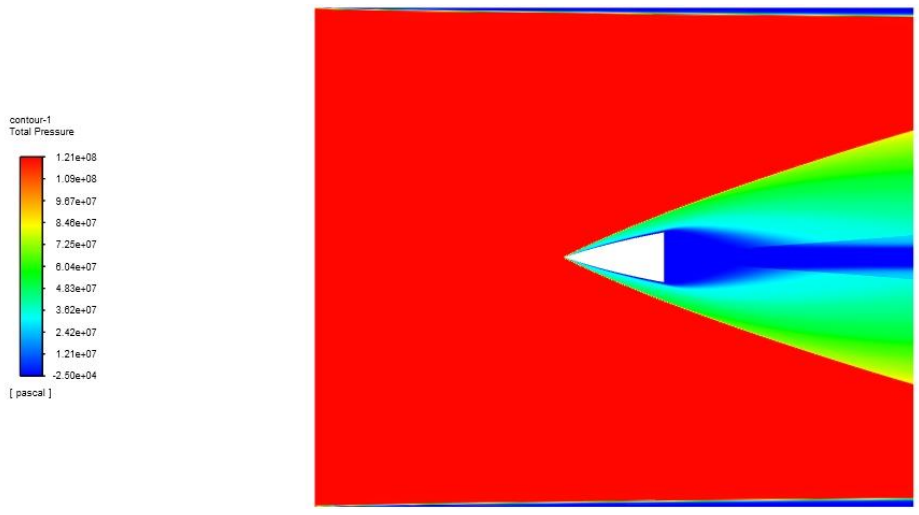

Figure 4.7 Pressure contour of parabolic nose.

From the snapshot in Figure 4.7 of pressure contour for parabolic nose, the sudden change in total pressure in front shock wave to behind the shock wave can be seen. Also, it is evident from the snapshot that this nose creates a weaker shock wave than previously discussed parabolic one. That weaker shock wave results in lower amount of drag which is the interest of this work.

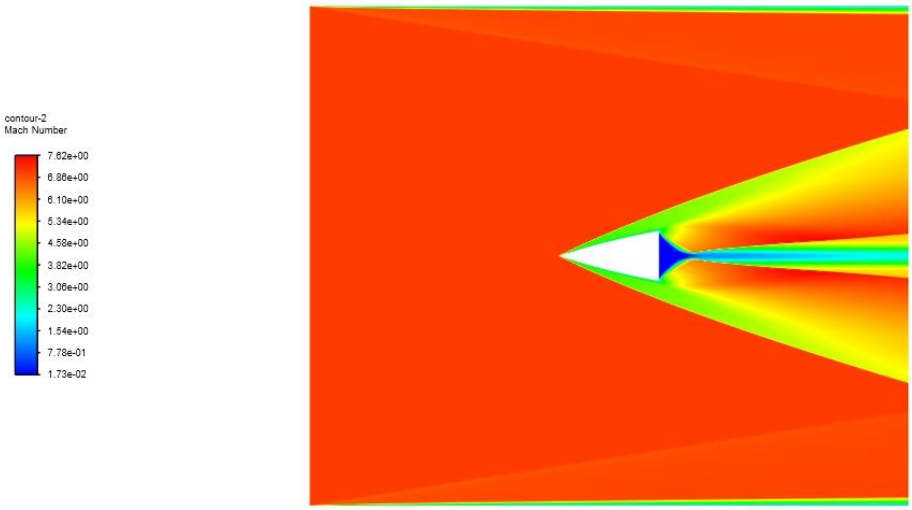

Figure 4.8 Velocity contour of parabolic nose.

From the snapshot in Figure 4.8 of velocity contour, the change in velocity from the front to behind can be seen in terms of Mach number for the bi-conic nose. It can be seen from the red zoned area in front of the shock wave that it contains a high amount of kinetic energy which contributes to the body heating.

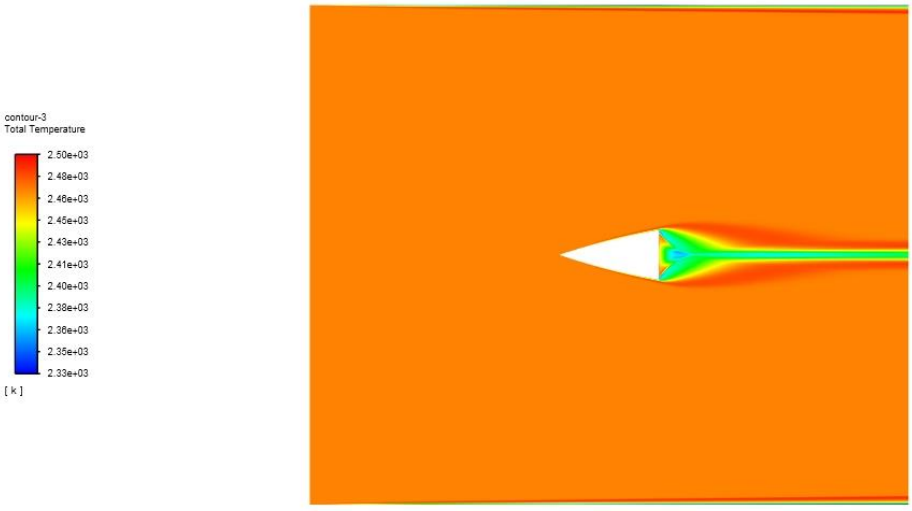

Figure 4.9 Temperature contour of parabolic nose.

From the snapshot in Figure 4.9 of total temperature contour obtained due to the flow over parabolic nose, it can be estimated that how much heat is being transferred to the body. The total temperature includes dynamic temperature which is a measure of kinetic energy contained by the freestream air. This kinetic energy than transformed into the thermal energy as air molecules passes through the shock wave.

4.4 Discussion

The obtained results of drag and heat transfer for bi-conic, elliptical and parabolic nose cone are summarized in the Table 4.7.

Table 4.7 Drag and heat transfer for different noses.

Nose type	Drag (N)	Heat flux(W/m^2)
Bi-conic	37634.47	281504.7
Elliptical	71580.91	712825.9
Parabolic	23820.51	257792

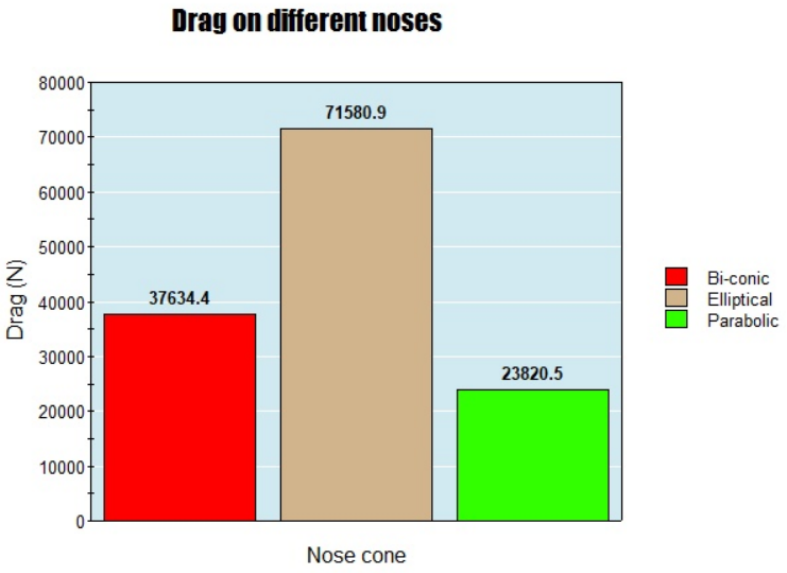

Figure 100 Drag of different noses shown in a bar chart.

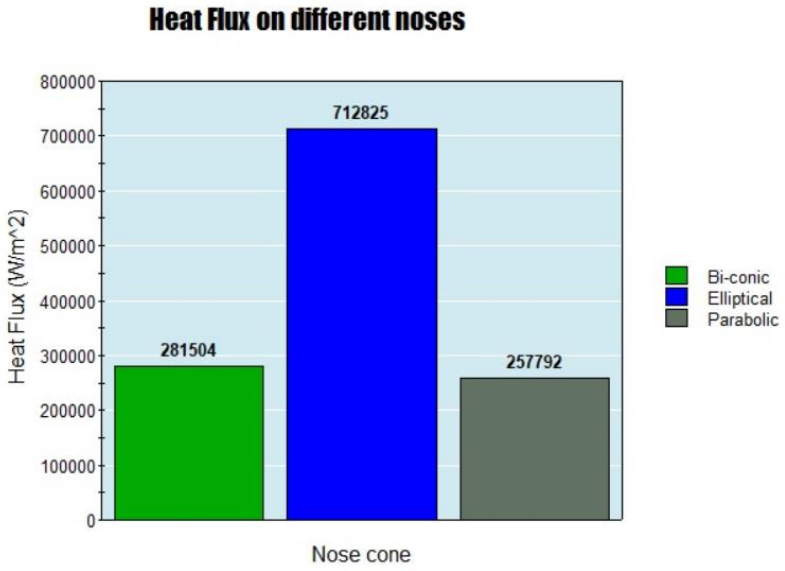

Figure 11 Heat Flux of different noses shown in a bar chart.

From the pressure contours of the elliptical nose, it can be seen that though the slender body of the nose produce a weaker shock wave which does increase the drag force but supposed to reduce the heat transfer but didn't. This could be due to the convective trend of the nose profile beyond frontal slenderness which may facilitate the heat transfer.

The problem incorporated with high magnitude of drag in elliptical nose is significantly dealt with in the bi-conic nose by creating a stronger shock wave. That strong shock wave creates a reduced amount of drag as it should but also should have increased the heat transfer. As the name represents, bi-conic has two conics with the one in the front being more diverged and the other at rear being less. The frontal one creates a stronger shock wave but with respect to the rear one it is a weak shock wave. It is like the frontal conic acts as a slender front for the rear one which also reduces the drag. The effects of these characteristics are evident in the result.

The parabolic nose is created by merging two symmetric cut-out parts of the upper portion of a parabola. That provides a pointy front to the nose profile creating a stronger shock wave thus reducing drag at a great amount. Since it is a cut-out part of a parabola, the slight convective trend of the nose profile diverges the upcoming air flow, reducing heat transfer to the body. As a result, it provides a better outcome than the bi-conic nose with reduced drag and heat transfer. Although it is safe to say that bi-conic nose with adjusted front conic could perform better than parabolic nose.

By comparing above shown results, we can come to the conclusion that elliptical nose is providing better performance than others.

Chapter 5
Conclusions

As it was mentioned earlier that the analysis if this work is limited into three nose shapes. After performing simulation on those nose shape under the condition of Mach 7.1 at an altitude of 10 km from the sea-level, the findings can be represented as below.

- Parabolic nose has shown best performance with lowest amount of drag of 23820.516 N and a heat flux of 257792 W/$\boldsymbol{m^2}$.
- Bi-conic nose has also shown good performance but not as parabolic nose. The amount of drag is 37634.47 N and the heat flux is 281504.7 W/$\boldsymbol{m^2}$. An educated guess could be made here that by varying the frontal cone dimensions like length and base diameter, a better result can be obtained.
- Elliptical nose shown the poorest performance which is beyond consideration with a drag of 71580.91 N and a heat flux of 712825.9 W/$\boldsymbol{m^2}$.

The scope of the future work of this study is very promising and could contribute to the real-world applications. For advanced analysis, some inclusion to the with the current ones could be made. Those are-

- Dissociated air chemistry model can be included for better results that includes air dissociation at high temperature.
- Different non-axisymmetric and real-life shapes could be analyzed.
- An optimization algorithm could be included required reduction in any of drag and heat transfer.

References

[1] J. D. Anderson, *Fundamentals of Aerodynamics*, McGraw-Hill, 6th Edition, 2017

[2] Seager, C., & Agarwal, R. (2017). Hypersonic Blunt-Body Shape Optimization for Reducing Drag and Heat Transfer. Journal of Thermophysics and Heat Transfer, 31, 48-55. https://doi.org/10.2514/1.T4650

[3] Hemateja, A., Teja, B., Kumar, A., & Rakesh, S. (2017). Influence of Nose Radius of Blunt Cones on Drag in Supersonic and Hypersonic Flows. IOP Conference Series: Materials Science and Engineering, 225. https://doi.org/10.1088/1757-899X/225/1/012045

[4] Liu, Y., & Jiang, Z. (2013). Concept of Non-Ablative Thermal Protection System for Hypersonic Vehicles. AIAA Journal, 51, 584-590. https://doi.org/10.2514/1.J051875

[5] Li, S., Huang, W., Lei, J., & Wang, Z. (2018). Drag and heat reduction mechanism of the porous opposing jet for variable blunt hypersonic vehicles. International Journal of Heat and Mass Transfer. https://doi.org/10.1016/J.IJHEATMASSTRANSFER.2018.06.054

[6] Mansour, K., & Khorsandi, M. (2014). The drag reduction in spherical spiked blunt body. Acta Astronautica, 99, 92-98. https://doi.org/10.1016/J.ACTAASTRO.2014.02.009

[7] Tahani, M., Karimi, M., Motlagh, A., & Mirmahdian, S. (2013). Numerical investigation of drag and heat reduction in hypersonic spiked blunt bodies. Heat and Mass Transfer, 49, 1369-1384. https://doi.org/10.1007/S00231-013-1173-4

[8] Meyer, B., Nelson, H., & Riggins, D. (2001). Hypersonic Drag and Heat-Transfer Reduction Using a Forward-Facing Jet. Journal of Aircraft, 38, 680-686.

[9] https://help.solidworks.com/2021/english/SolidWorks/cworks/c_mesh_quality_checks.htm (DOA: 17 March,2024)

[10] https://www.engmorph.com/mesh-quality-parameters (DOA: 17 March,2024)

[11] https://www.engineeringtoolbox.com/standard-atmosphere-d_604.html (DOA: 17 March,2024)

[12] https://ntrs.nasa.gov/citations/19850004005

[13] Narayan, Ashish and Kumar, Sanjay and Pal, Pramod Kumar and Pandey, Shubham Kumar and Hansdah, Hirawati and., Ashok Kumar, Hypersonic Flow Past Over an Elliptic Nose Cone Configurations: International Conference on Recent Trends in Artificial Intelligence, IOT, Smart Cities & Applications (ICAISC-2020) (June 7, 2020).

[14] Narayan, A., Narayanan, S., & Kumar, R. (2017). Hypersonic flow past nose cones of

different geometries: a comparative study. SIMULATION, 94(8), 665–680.

Appendices

Appendix-A

Cost Estimation of the Project:

Items	Cost (Taka)
Materials: i)	
ii)	

Appendix-B

Work/Activities Plan of the project/thesis using Gantt chart:

Work/ Activities	Week 1	Week 2	Week 3	Week 4	Week 5	Week 6	Week 7	Week 8	Week 9	Week 10	Week 11	Week 12	Week 13	Week 14-26
Study of the research paper														
Finding the research gap														
Fixing the objectives and research methodology														
Writing the project proposal														
Presenting an proposal														
Develop the design/process														
Formulations and evaluations														
Results analysis														
Writing thesis														
Thesis correction and presentation preparation														

Final thesis presentation														

Appendix-C

Originality Report by Turnitin Plagiarism Software

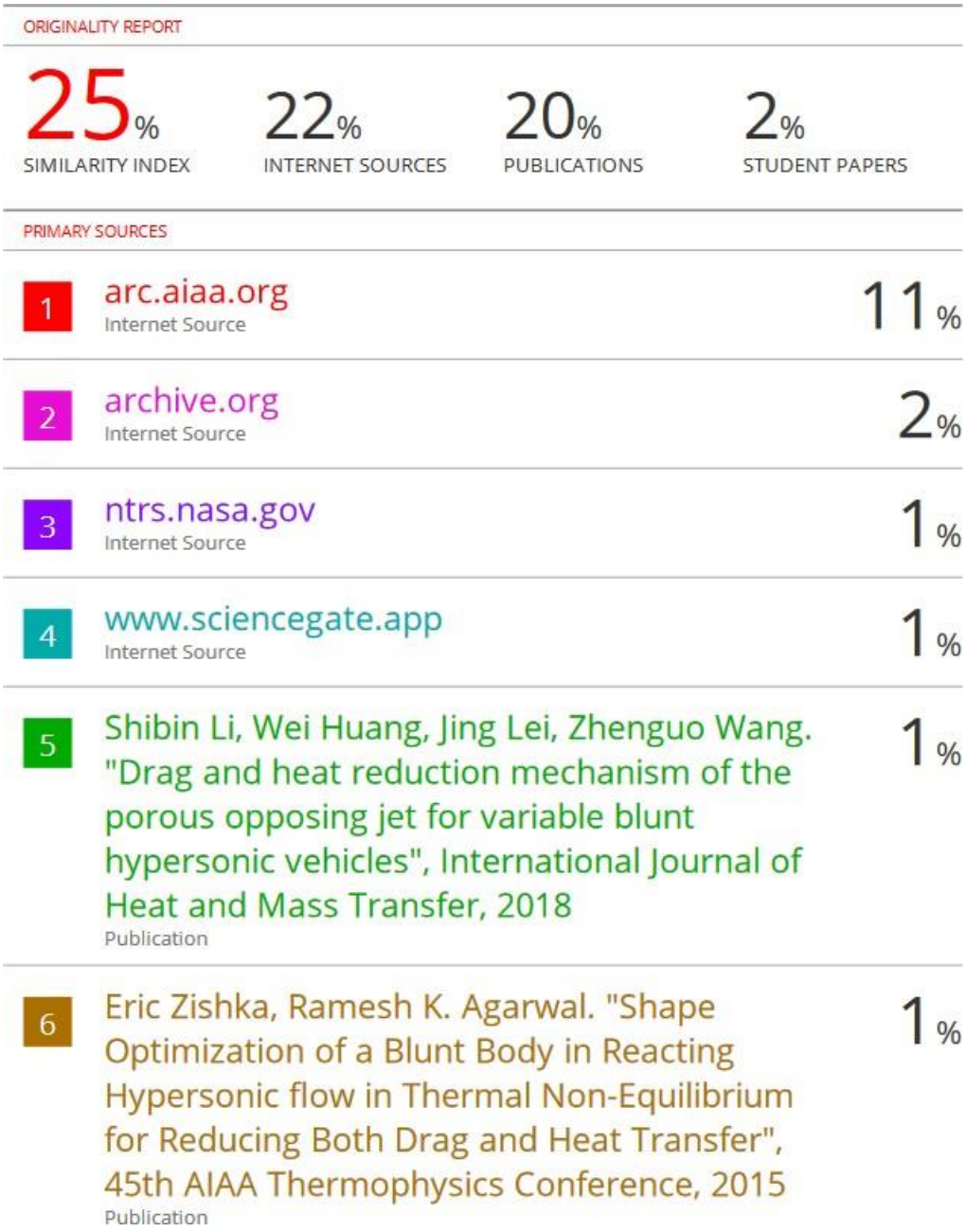

ORIGINALITY REPORT

25%	22%	20%	2%
SIMILARITY INDEX	INTERNET SOURCES	PUBLICATIONS	STUDENT PAPERS

PRIMARY SOURCES

1	arc.aiaa.org Internet Source	11%
2	archive.org Internet Source	2%
3	ntrs.nasa.gov Internet Source	1%
4	www.sciencegate.app Internet Source	1%
5	Shibin Li, Wei Huang, Jing Lei, Zhenguo Wang. "Drag and heat reduction mechanism of the porous opposing jet for variable blunt hypersonic vehicles", International Journal of Heat and Mass Transfer, 2018 Publication	1%
6	Eric Zishka, Ramesh K. Agarwal. "Shape Optimization of a Blunt Body in Reacting Hypersonic flow in Thermal Non-Equilibrium for Reducing Both Drag and Heat Transfer", 45th AIAA Thermophysics Conference, 2015 Publication	1%

Appendix-D

(This part will be filled/checked by the supervisor)

CO-PO-K-P-A Mapping

PO1	**Engineering knowledge:** Apply the knowledge of mathematics, science, engineering fundamentals, and an engineering specialization to the solution of complex engineering problems.
PO2	**Problem analysis:** Identify, formulate, research literature, and analyze complex engineering problems reaching substantiated conclusions using first principles of mathematics, natural sciences, and engineering sciences.
PO3	**Design/development of solutions:** Design solutions for complex engineering problems and design system components or processes that meet the specified needs with appropriate consideration for the public health and safety, and the cultural, societal, and environmental considerations.
PO4	**Conduct investigations of complex problems**: Use research-based knowledge and research methods including design of experiments, analysis and interpretation of data, and synthesis of the information to provide valid conclusions.
PO5	**Modern tool usage:** Create, select, and apply appropriate techniques, resources, and modern engineering and IT tools including prediction and modeling to complex engineering activities with an understanding of the limitations.
PO6	**The engineer and society:** Apply reasoning informed by the contextual knowledge to assess societal, health, safety, legal and cultural issues and the consequent responsibilities relevant to the professional engineering practices.
PO7	**Environment and sustainability:** Understand the impact of the professional engineering solutions in societal and environmental contexts, and demonstrate the knowledge of, and need for sustainable development.
PO8	**Ethics:** Apply ethical principles and commit to professional ethics and responsibilities and norms of the engineering practice.
PO9	**Individual and team work:** Function effectively as an individual, and as a member or leader in diverse teams, and in multidisciplinary settings.
PO10	**Communication:** Communicate effectively on complex engineering activities with the engineering community and with society at large, such as, being able to comprehend and write effective reports and design documentation, make effective presentations, and give and receive clear instructions.
PO11	**Project management and finance:** Demonstrate knowledge and understanding of the engineering and management principles and apply these to one's own work, as a member and leader in a team, to manage projects and in multidisciplinary environments.

PO12	**Life-long learning:** Recognize the need for, and have the preparation and ability to engage in independent and life-long learning in the broadest context of technological change.